

Chapter 7.

Excited-state Dynamics of Aromatic Carbonyls

The aromatic carbonyl molecules, exemplified by benzaldehyde and acetophenone, have been of experimental interest for decades. Both benzaldehyde and acetophenone possess a complex manifold of $n\pi^*$ and $\pi\pi^*$ excited states in both singlet and triplet manifolds resulting in simultaneous and competitive photophysical and photochemical decay processes upon excitation. These molecules are ideally suited for the study of the physical processes of intersystem crossing and phosphorescence, as well as reactions of valence isomerization, bond breakage, and atom transfer.

Ambiguities abound in the pathways, products, and time scales. The mechanisms by which S_2 excited benzaldehyde yields molecular dissociation products while excited acetophenone homolytically cleaves are important issues that portend major advances in understanding excited-state decay processes. This chapter is a compilation and expansion

of the results reported in three papers on the photochemistry and photophysics of benzaldehyde and acetophenone.¹ It is organized as follows: Section 7.1 reviews the spectroscopic literature of benzaldehyde and acetophenone. Section 7.2 describes experimental and theoretical conditions as they differ from the standards described in Chapter 3. Section 7.3 presents the results of the UED studies on both molecules following 266.7 nm femtosecond excitation to their S_2 states. Section 7.4 discusses the deduction of the mechanisms and the significance of these findings.

7.1 Review of the spectroscopic literature

7.1.1. The photophysics and photochemistry of benzaldehyde

The absorption spectrum of vapor-phase benzaldehyde with wavelengths longer than 260 nm shows two broad peaks. The lower peak is highly structured and corresponds to a transition to the S_1 ($n\pi^*$) state. The higher-energy peak, marking the transition to the S_2 ($\pi\pi^*$) state, is much more intense and shows only weak structure.² Absorption into either of these states, and the S_3 ($\pi\pi^*$) that lies above, results in phosphorescence.^{3,4} This particular feature of benzaldehyde has been exploited by numerous studies attempting explanation of its photophysics. Experiments to this end have been performed on benzaldehyde in vapor,²⁻¹⁹ in solution,²⁰ and in matrices.²¹⁻²³

The proximity and nature of low-lying $n\pi^*$ and $\pi\pi^*$ states of both singlet and triplet manifolds have been a main focus both experimentally and theoretically. The origin of S_1 ($n\pi^*$) was found to lie 26,919 cm^{-1} above the ground state by sensitized phosphorescence⁷ and 26,920 cm^{-1} above by sensitized surface electron ejection.¹⁸ It is

slightly blue-shifted in hexane solution ($26,960\text{ cm}^{-1}$)²⁰ and in p-dibromobenzene matrices ($27,284\text{ cm}^{-1}$).²⁴ S_2 ($\pi\pi^*$) has its origin at $35,200\text{ cm}^{-1}$ and $35,191\text{ cm}^{-1}$ relative to the ground state as seen in the phosphorescence excitation spectrum¹⁰ and ionization excitation spectrum,¹² respectively. Another $\pi\pi^*$ state, S_3 , has its 0-0 transition at $41,334\text{ cm}^{-1}$ as noted by UV absorption.²⁵ In the triplet manifold, matters are more complex since the $n\pi^*$ and $\pi\pi^*$ states are very close lying. Emission in the vapor is detected only from the $n\pi^*$ (T_1), however in certain matrix environments the $\pi\pi^*$ may be shifted lower in energy allowing direct spectral observation. The T_1 origin in the vapor phase is readily distinguished by phosphorescence and is assigned between $25,180$ and $25,190\text{ cm}^{-1}$.^{7,8,16-18} Similar to values for the S_1 origin, values for T_1 in liquid hexane²⁰ and in a p-dibromobenzene matrix²⁴ are blue-shifted to $25,195$ and $25,515\text{ cm}^{-1}$, respectively. Some band congestion in the vapor phosphorescence spectrum $\sim 1000\text{ cm}^{-1}$ above the T_1 origin is cautiously assigned to intensity borrowing by the T_2 ($\pi\pi^*$) state.^{7,8,16,18} The caution in this assignment arises due to theoretical suggestion that the spacing between the levels is, in fact, large enough not to cause significant breakdown of the Born-Oppenheimer approximation.^{11,17,26} Theory places the T_1 - T_2 energy gap between 726 and 4190 cm^{-1} depending on the method of calculation.²⁷⁻³⁰ In matrices, however, the $^3n\pi^*$ and $^3\pi\pi^*$ levels switch and both are observed; the $\pi\pi^*$ state is lower by 162 to $\sim 2000\text{ cm}^{-1}$ and varies highly with the choice of host.^{22,24}

Decay of the excited-state population by phosphorescence is the most widely known relaxation pathway in gas-phase benzaldehyde and the quantum yield of emission approaches unity when excitation is near the S_1 origin.¹⁴ It continues to be observed,

albeit with less intensity, as excitation reaches the S_3 state. Two conflicting reports of the phosphorescence behavior at higher excitation energies exist in the literature. In several accounts it is reported that drop-offs in yield occur near both the S_2 and S_3 thresholds.^{4,6,11,15} Yet in another account, the drop-offs are refuted as gas-cell “wall effects” and simply a monotonic decrease is reported.³ Independent of the exact behavior, a non-radiative channel depleting the excited-state population becomes important above S_1 excitation making phosphorescence less significant. An intermediate state invoked in the non-radiative decay route lives long enough for collision-induced deactivation as added gas causes an increase in phosphorescence yield.^{6,10,11,13,15} The phosphorescent state itself is found to live in the range of ns to ms, becoming shorter-lived with increased excess energy.^{3,9,13,18} Lifetime information is also available for the S_2 state by femtosecond photoelectron spectroscopy. It was observed to live for 440 fs at the origin and undergoes a monotonic lifetime decrease with increasing excitation energy, leaving the state by ultrafast internal conversion.¹⁹

The structures of the electronic states of benzaldehyde are largely obtained through theoretical means²⁸⁻³⁰ with some experimental exceptions. The ground state has been studied by both microwave spectroscopy³¹ and electron diffraction³² in the gas phase, and the barrier to formyl group torsion is found to be 1715 cm^{-1} and $>1700\text{ cm}^{-1}$, respectively. Additionally, analysis of the phosphorescence spectra and S_1 excitation spectra shows the C=O stretch as the most intense band with prominent progression, confirming the $n\pi^*$ nature of both states as well as their structural similarity to the ground state (except for the C=O length).⁷

In addition to the rich photophysics studied in this molecule, there exist chemical pathways resulting in radical and molecular dissociation products. The first thorough experiments on the photochemistry of benzaldehyde¹⁰ show dissociation into benzene and carbon monoxide upon photolysis by 276 nm radiation (S_2 excitation). The products were extracted from the cell and identified by gas chromatography. Being relatively insensitive to added oxygen, the molecular dissociation products are determined to have formed through a “concerted” reaction and not through radical intermediates. At low pressures the quantum yield of benzene is found to be 0.89, and the addition of foreign gases causes the benzene yield to decrease while increasing the yield of phosphorescence. A model is proposed with short and long benzene-formation channels, the long channel may be deactivated to the phosphorescent state (T_1) by collisions.¹⁰ An insensitivity to collisions with added O_2 further supports the non-radical nature of the reaction, as the yield of benzene was unchanged.⁵ The nature of the reaction was conclusively verified in experiments where benzaldehyde- d_6 was mixed with benzaldehyde- h_6 and photolyzed with 276 nm radiation.¹¹ Only the “concerted” intramolecular reaction products benzene- d_6 and benzene- h_6 were identified. Yield of the dissociation products was near unity.¹¹ Benzene ions have also been detected in mass spectrometry experiments pumping at 248 nm.³³

Although ultrafast dynamics was hitherto lacking, some time-scales of benzene formation have been obtained. In an ionization experiment using single shots of 2 ns pulses,³⁴ benzene ions were detected with 258.9 nm excitation but not with 258.7 nm. For both excitations benzene is formed within the pulse, but because ground-state benzene

has a resonant absorption at 258.9 nm, but not at 258.7 nm, it is efficiently ionized and observed at 258.9 nm. Furthermore, the photoelectron spectrum was recorded at both excitation energies for benzaldehyde as well as benzene. No photoelectrons were detected at 258.7 nm, but the spectrum observed using 258.9 nm matched that of ground state benzene. In addition to confirmation of the product, these experiments put an upper-bound of 2 ns on the photoreaction.³⁴ In another report, single shots at 266 nm showed no benzene ion signal when the pulsewidth was 25 ps, but showed a near-unity production of benzene ions when the excitation laser pulsewidth was 8 ns.^{35,36}

Using 10 ns pulses at 266 nm in a mass spectrometer Polevoi *et al.* determined the time constant for benzene ion formation to be ~ 30 ns. Their kinetic model predicts that the reaction corresponds to triplet benzaldehyde dissociating into benzene in its own triplet state and ground state carbon monoxide.³⁷ The most recent work on benzaldehyde photochemistry by Silva and Reilly, a time-resolved mass spectrometry study using 3–5 ns pulses, contributes valuable additional information.³⁸ With excitation into S_2 and time delayed photoionization by a 157 nm probe laser, both benzene and parent benzaldehyde ions are detected. The ratio of benzene to benzaldehyde ions increases with decreasing excitation wavelength – complete dissociation occurring near 260 nm excitation. Two decay times are observed for the benzaldehyde ion: a short decay of <1 μ s and a longer decay of >1 μ s. The shorter decay time nearly coincides with the time constant of benzene ion appearance and is ~ 80 ns at 270 nm excitation. Since the probe pulse (157 nm) is only intended to ionize electronically excited benzenes, the benzene ion signal is believed to be from the triplet. However, ground state benzene is also identified in their

results by its photoionization excitation spectrum and must be formed via a different pathway. The threshold for benzene formation is placed somewhere near (but below) the S_2 origin.³⁸

Radical products were reported only once from S_2 , after gas-phase photolysis of benzaldehyde by 7 ns pulses of 280, 285, and 308 nm radiation. HCO radicals were detected by absorption and quantum yields were estimated at 0.3 to 0.4.³⁹ Based on the evidence in numerous previous works, the radicals must surely be products of a multi-photon reaction. The chemistry observed upon excitation into the S_2 state contrasts with the different chemistry observed through S_1 . Several researchers report no chemistry at all after S_1 excitation.^{3,11,13,35,36} Chemistry that is reported is of a fragmentary nature resulting in the benzoyl radical and atomic hydrogen.^{21,40} One account notes a slow build up of polymer on the walls of the gas cell after prolonged exposure at 328 or 365 nm.¹⁰ Hydrogen atoms were also produced in the thermal breakdown of benzaldehyde above 1000 K. CO may also be lost from the resulting fragment above 1150 K.⁴¹

7.1.2. The photophysics and photochemistry of acetophenone

The states of acetophenone are similarly ordered as benzaldehyde, with two closely lying triplet states (the lower one being strongly phosphorescent) located just below the S_1 origin. There are many experimental measurements and theoretical estimates of the relative energies of the states in the gas phase. S_1 ($n\pi^*$) is found to lie 27,279 cm^{-1} above S_0 by its sensitized phosphorescence.⁷ The origin of the S_2 ($\pi\pi^*$) excitation spectrum is 35,402 cm^{-1} above S_0 ⁴² and the 0-0 by opto-acoustic spectroscopy is reported at 34010 cm^{-1} .⁵ The S_3 ($\pi\pi^*$) origin is seen at 41,695 cm^{-1} by absorption in a jet.²⁵ In the triplet

manifold, the well-known T_1 ($n\pi^*$) state has its origin at $25,791\text{ cm}^{-1}$ by sensitized phosphorescence⁷ and $25,786\text{ cm}^{-1}$ by its direct emission.⁴³ Like benzaldehyde, the T_2 ($\pi\pi^*$) state was not directly observed in the vapor. A congestion of spectral features noted 600 cm^{-1} above the T_1 origin has been attributed to possible mixing with the nearby T_2 .⁷ In general, the vapor phase spectrum is weaker than that of benzaldehyde, with a less prominent progression of the carbonyl stretching bands – perhaps from a greater contribution of $\pi\pi^*$ character.⁸ Unlike benzaldehyde, emission from only a single phosphorescent site is observed in certain matrices and believed to correspond to some highly perturbed state. Indeed, the spectrum shows features from both states precluding it from being unequivocally assigned to either the $^3n\pi^*$ or $^3\pi\pi^*$. The conclusion is that the T_1 – T_2 energy gap is even less than that of benzaldehyde.^{22,43} The energies and geometries of these low-lying electronic states have been studied theoretically, yielding similar results. An estimate of the T_1 – T_2 energy gap is only 565 cm^{-1} .^{29,30}

Like for benzaldehyde, the prolific study of acetophenone is largely due to its intense phosphorescence facilitated by efficient intersystem crossing from S_1 into the triplet manifold. The photophysics of acetophenone have been studied in the gas phase,^{5-8,19,25,42-46} solution,^{20,47} and in matrices.^{21,22,43} Phosphorescence detected in the vapor phase is seen to decrease in intensity with increasing photon energy and exhibits a drop-off as excitation approaches S_2 . The phosphorescence quantum yield at the S_1 origin is near unity^{6,44,46} while at the S_2 origin it is reduced to $\sim 10^{-4}$.⁴² The drop-off is attributed to the rise of an intermediate state that can be collisionally deactivated – increased phosphorescence yield is observed with the addition of foreign gas.^{6,44,46} A kinetic model

predicts a lifetime of 380 ns for the intermediate.⁶ Again, like benzaldehyde, the presence of a drop-off is contested with contrary evidence depicting a monotonic decrease.⁴⁶

Although phosphorescence lifetimes are known to be in the μs -ns range, the lifetimes of other states have gone largely unmeasured. By linewidth measurements the lifetime of the S_2 origin is found to be 260 fs⁴² and a subsequent femtosecond time-resolved photoelectron experiment put it at 140 fs, faster than that of benzaldehyde. The faster decay is likely the consequence of more efficient radiationless relaxation mediated by extra accepting modes from the methyl group.¹⁹ The lifetime of the Rydberg state reached by 193 nm absorption is instrument limited and <200 fs.⁴⁸ These fast lifetimes and the experimentally known (and theoretically predicted)²⁹ efficiency of intersystem crossing are consistent with the lack of fluorescence from acetophenone. Fluorescence has been observed, however, from acetophenone derivatives in solution with attached aromatic groups.⁴⁹

Experimental information regarding the structures of the excited states is confined to the S_1 and T_1 states. The carbonyl stretching progression observed is indicative of $n\pi^*$ states with the main structural difference from the ground state being a lengthening of the C=O bond.⁷ Experimental information on the $\pi\pi^*$ structures is limited to acetophenone derivatives where the $^3\pi\pi^*$ state is lower in energy. Substituted acetophenones were excited in solution with 266 nm light after which (500 ns) infrared spectra were recorded. The changes in the spectrum indicate a structural difference with the ground state mainly in the aromatic ring consistent with the quinoid structure of a $\pi\pi^*$ state.⁵⁰ Theoretical inquiries backup these experimental results reaffirming structural differences with the

ground state localized in the C=O bond for $n\pi^*$ states and in the aromatic ring for $\pi\pi^*$ states.^{29,30} It is to be noted that no experimentally determined structure exists for ground state acetophenone.

Acetophenone photochemistry has attracted less interest than that of benzaldehyde. Unlike the molecular dissociation seen in the aldehyde, radical products represent the photochemistry of this aromatic ketone. Carbon monoxide was not detected in the earliest of experiments by Berger and Steel.⁴⁴ Instead, the major products are the benzoyl and methyl radicals observed at multiple excitations ranging from 282 nm to 193 nm and also seen as products in strong-field dissociation experiments. The other radical cleavage products, phenyl and acetyl radicals, are also observed but with a much lower yield.^{44,51,52} Like benzaldehyde, the yield of chemical products is seen to approach unity with S_2 excitation at the lowest pressures but decreases coincident with increasing phosphorescence when foreign gas is added, suggesting a vibrationally excited intermediate to fragmentation. Only trace amounts of the molecular dissociation products of carbon monoxide and toluene were detected after photolysis by 193 and 248 nm radiation a branching ratio with the radical products of $\sim 1:100$.⁵² Little to no decomposition products are noted upon S_1 (365 nm) excitation.⁴⁴

7.2 Experimental and theoretical details

See Chapter 3 for a detailed account of the apparatus. Here only specific conditions will be described. Samples used in these experiments were obtained from Aldrich: acetophenone (99%), benzaldehyde (99.5+ %), and 1,3-butadiene (>99%), and

Air Liquide: carbon dioxide (99.5%) and xenon (99.995%). All samples were used without further purification.

The electron pulse properties for these experiments were 8.5×10^4 electrons/pulse with ~ 17 ps pulsewidth for acetophenone, and 2.6×10^4 electrons/pulse with ~ 4 ps pulsewidth for benzaldehyde. The FWHM of the electron beams, w_e , was measured to be 370 μm and 360 μm for benzaldehyde and acetophenone, respectively. The FWHM of the molecular beams, w_m , was measured to 380 μm for benzaldehyde and 270 μm for acetophenone. The laser beam width, w_l , at the interaction region was taken to be ~ 350 μm based on the focal properties of the lens before the inlet window.

For benzaldehyde the temperatures of the nozzle, manifold, and sample were 210 $^\circ\text{C}$, 230 $^\circ\text{C}$, and 129 $^\circ\text{C}$, respectively. The temperature of the sample reservoir was increased to 148 $^\circ\text{C}$ over the course of the experiment in order to keep constant the pressure and the dependent scattering signal. For acetophenone the temperatures of the nozzle, manifold, and sample were 230 $^\circ\text{C}$, 260 $^\circ\text{C}$, and 110 $^\circ\text{C}$, respectively, and the sample temperature was increased to 120 $^\circ\text{C}$ during this much shorter experiment.

The time-zero lensing measurements for both experiments were clearly defined. For example, the electron beam lensing properties as measured in the calibration stages of the acetophenone experiment are shown in Fig. 7-1.

Using the abovementioned beams' properties and the formulae described in Section 3.2.6, the overall time resolutions of the benzaldehyde and acetophenone experiments were calculated to be 5 ps and 17 ps, respectively.

One hundred diffraction patterns (4 minute exposures at 1 kHz laser and electron beam repetition rates) were taken for each of: background electron scattering (no molecular beam), carbon dioxide, xenon, ground state (molecular sample without excitation laser), each time-resolved benzaldehyde data point (−100 ps, −50 ps, −10 ps, −5 ps, +0 ps, +5 ps, +10 ps, +15 ps, +20 ps, +30 ps, +40 ps, +50 ps, +100 ps, +1000 ps), and each time-resolved acetophenone data point (−100 ps, +50 ps, +100 ps). Only three points were taken for acetophenone because it had a propensity to coat the inlet window and drastically reduce the amount of excitation laser reaching the interaction region. It was found that three time points could be taken before reduced laser flux caused the difference signal to become too small to analyze.

For all results presented herein, the camera length was measured independently by recording electron diffraction data from carbon dioxide (see Section 3.2.7). For the studies presented here, the camera distances were determined to be 13.38 cm (benzaldehyde experiment) and 13.42 cm (acetophenone experiment).

Initial guess geometries for the possible reaction products of the photolysis of the two aromatic carbonyls were obtained from quantum chemical calculations (see Section 4.5.1). Geometry optimization for the ground state of reactants and possible products of benzaldehyde and acetophenone systems were carried out at the B3LYP level using the 6-311G(d,p) basis set. UB3LYP/6-311G(d,p) was used for radical product candidates such as those involving H, methyl, formyl, acetyl, benzoyl, and phenyl radicals as well as for the triplet state of molecules. Planar symmetry was imposed for the singlet ground states of benzaldehyde and acetophenone and the T_1 state of benzaldehyde, and frequency

calculations were performed to ensure minimum energy configurations. For the T_1 state of acetophenone, the symmetry constraint was lifted, since the methyl orientation deviates from planar symmetry; the skeleton remains nearly planar. The theoretically determined relative energies of the parent and product molecules are listed in Table 7-1 and compared to experimental values where available; agreement is satisfactory. Experimental values of the changes in heats of formation at 298 K were taken from NIST⁵³ and then converted to 0 K values using the theoretical frequencies obtained from DFT calculations.

Table 7-1. Theoretical and experimental energetics of some possible products of benzaldehyde and acetophenone photolysis.

Molecule	Channel	Energy (cm^{-1})		$T_B^{\text{Max c}}$ (K)
		Theoretical ^a	Experimental ^b	
benzaldehyde	$\text{C}_6\text{H}_5\text{CHO} (S_0^*)$	0	0	2379
	$\text{C}_6\text{H}_5\text{CHO} (T_1)$	23015	25183	1307
	$\text{C}_6\text{H}_5\text{CHO} (T_2)$	25148	25183~26183	1161
	$\text{C}_6\text{H}_6 (S_0) + \text{CO}$	840	460	2696
	$\text{C}_6\text{H}_6 (T_1) + \text{CO}$	30489	30087 ^d	1044
	$\text{H} + \text{C}_6\text{H}_5\text{CO}$	30403	n/a ^f	954
	$\text{C}_6\text{H}_5 + \text{HCO}$	32335	34637	993
	acetophenone	$\text{C}_6\text{H}_5\text{COCH}_3 (S_0^*)$	0	0
$\text{C}_6\text{H}_5\text{COCH}_3 (T_1)$		23569	25791	1157
$\text{C}_6\text{H}_5\text{COCH}_3 (T_2)$		25643	n/a ^f	1068
$\text{C}_6\text{H}_5\text{CH}_3 (S_0) + \text{CO}$		1860	1814	2227
$\text{C}_6\text{H}_5\text{CH}_3 (T_1) + \text{CO}$		30662	30890 ^e	945
$\text{CH}_3 + \text{C}_6\text{H}_5\text{CO}$		26660	n/a ^f	1284
$\text{C}_6\text{H}_5 + \text{CH}_3\text{CO}$		31200	34266	972

a) Theoretical energies were evaluated from B3LYP/6-311G(d,p) level calculations, except for the energies of the T_2 states of benzaldehyde and acetophenone, which were evaluated using MCSCF(10,9)/6-311G(d,p).

b) Experimental values were evaluated from the change in the heat of formation at 298 K⁵³ and converted to the 0 K value using DFT frequencies.

c) Temperatures for dissociation products are upper limits where all the excess energy is partitioned into vibrational modes (see Section 4.5.4).

d) The energy of C_6H_6 ($^3\text{B}_{1u}$) is $29627 \pm 12 \text{ cm}^{-1}$ by MATI of discharged benzene.⁵⁴ The energy of C_6H_6 ($^3\text{B}_{1u}$) is 3.665 eV from EEL data.⁵⁵

e) The energy of $\text{C}_6\text{H}_5\text{CH}_3$ (T_1) is 3.605 eV (0-0) for the solid,⁵⁶ and 3.8 eV (maximum) for the gas.⁵⁷

f) These data were not available.

MCSCF calculations were performed for the singlet and triplet, ground and excited states of benzaldehyde and acetophenone to explore structural changes during photophysical processes. An active space was chosen to account for the carbonyl $\pi^* \leftarrow n$ and phenyl $\pi^* \leftarrow \pi$ transitions in both molecules. Specifically, ten electrons were partitioned into nine orbitals: one oxygen nonbonding orbital, one each of C=O π and π^* orbitals, and three each of C=C π and π^* orbitals. The 6-31G(d) basis set was used to reproduce previous work on benzaldehyde by Wang *et al.*³⁰ Following this confirmation, calculations were then conducted using the 6-311G(d,p) basis set. The initial molecular orbitals were guessed from the B3LYP calculations with virtual orbital optimizations after SCF convergence. Using the guessed orbitals, which were properly reordered to form the nine active-space orbitals, vertical energies were calculated and molecular orbital characters were visually checked to confirm the corresponding transitions observed in the experiments. Full structural optimizations were followed by vibration frequency calculations to check the effect of imposing planar symmetry. Multi-reference perturbation corrections (MCQDPT)⁵⁸ were applied to evaluate the electron correlation energies. Relative energies of excited states are listed in Table 7-2 and compared with experimental values where available.

Table 7-2. Theoretical and experimental energetics of the benzaldehyde and acetophenone excited states

	Benzaldehyde			Acetophenone		
	Experiment ^a	MCSCF ^b	MCQDPT ^b	Experiment ^c	MCSCF ^b	MCQDPT ^b
S ₀	0	0	0	0	0	0
S ₁	(¹ nπ*)	26921	26541	27279	-	-
					(26703) ^d	(27278) ^d
S ₂	(¹ ππ*)	35191	35978	35402	36074	33329
T ₁	(³ nπ*)	25183	24844	25791	25556	25622
			(24766) ^d		(25542) ^d	(25514) ^d
T ₂	(³ ππ*)		24821		25102	25643
T ₃	(³ ππ*)				36361	32639

a) For benzaldehyde, the S₁ origin is 26919 cm⁻¹,⁷ 26920 cm⁻¹,¹⁸ and 26921 cm⁻¹.¹⁶ The S₂ origin is 35200 cm⁻¹,¹⁰ and 35191 cm⁻¹.¹² The S₃ origin is 41334 cm⁻¹.²⁵ The T₁ origin is 25180 cm⁻¹,¹⁷ 397 nm,⁹ 25184 cm⁻¹,⁸ 25183 cm⁻¹,⁷ 397 nm,¹⁸ and 25183 cm⁻¹.¹⁶

b) MCSCF and MCQDPT calculations were performed using the 6-311G(d,p) basis set and an active space of ten electrons partitioned in nine orbitals.

c) For acetophenone, the S₁ origin is 27279 cm⁻¹.⁷ The S₂ origin is 35402 cm⁻¹,⁴² and 34010 cm⁻¹.⁵ The S₃ origin is 41695 cm⁻¹.²⁵ The T₁ origin is 25791 cm⁻¹,⁷ and 25786 cm⁻¹.⁴³

d) Values in parenthesis are for structures where planar symmetry was imposed resulting in an imaginary frequency.

In calculating reactive pathways from the nπ* S₁ excited state of benzaldehyde, the SCF suffered convergence failure; the selected initial guess wavefunctions do not remain effective when large nuclear coordinate changes are implemented.⁵⁹ For unknown reasons, preparing the initial guess vector at the rearranged geometry was also unsuccessful. Since the S₁ MCSCF reaction pathway calculations failed, UB3LYP/6-311G(d,p) was employed to study the reaction on the nπ* T₁ surface instead. Both the S₁ ¹nπ* and T₁ ³nπ* states of acetophenone and benzaldehyde have nearly identical stationary geometries and vibrational frequencies. The similarities permit results found for T₁ benzaldehyde to be carefully adapted to the S₁ surface; a correction of 3906 cm⁻¹ is used – the difference between the experimental S₁ origin and the DFT T₁ origin. Later discussion of the S₁ dynamics is made under the assumption that calculations on T₁ provide information relevant to its singlet counterpart.

7.3 Experimental results

7.3.1. The time-resolved structures of benzaldehyde

Fig. 7-2 shows the two-dimensional frame-referenced difference patterns for benzaldehyde at 483 K obtained by subtracting the reference pattern (an average of the -100 , -50 , and -10 ps ratio patterns) from the ratio patterns of the other time points. The appearance of diffraction rings in the patterns signifies a structural change between the parent structure (at -100 ps) and the structures formed as a result of the excitation pulse at time-zero. The increase in magnitude of structural change with time is readily seen in the time dependent data. The same features are retained over time, but only increase in amplitude, signifying the growth in population of a common product structure throughout. This can be further seen in Fig. 7-3 which plots the raw time-resolved data – $R^N(\text{pix})$ in Eq. (4-9), or more accurately, $\Delta R^N(\text{pix})$. The difference data point at $+50$ ps was selected for the refinement of the theoretical model on the basis of signal quality. The data from $s = 3.1 - 13.9 \text{ \AA}^{-1}$ were used, also owing to superior signal quality.

Table 7-3. The fraction fits of the various product channels

Product	Fraction (%)	χ^2	R
Hot benzaldehyde (2500 K)	9.09 ± 5.49	4.074	0.668
Benzene + CO	8.35 ± 6.95	4.824	0.787
Phenyl + formyl radicals	8.25 ± 5.97	6.098	0.930
Benzoyl + H radicals	18.78 ± 11.07	5.002	0.840
Benzene (T_1) + CO	8.32 ± 2.49	4.247	0.448
Benzaldehyde T_1	0.64 ± 5.71	10.679	24.976
Benzaldehyde S_1	1.29 ± 4.40	10.606	9.228
Benzaldehyde T_2	7.69 ± 4.31	5.722	1.016

Error bars are 3σ from the UED_2004 program.

Quantum chemical calculations were performed to arrive at suitable starting geometries for structural refinement. Such trial models were based on the various molecules proposed in the literature as products of benzaldehyde photochemistry and the

geometries of relevant excited states (see Section 7.1). The structural schematics for the possible product molecules are shown in Fig. 7-4. The actual products of photoexcitation were determined by comparing the +50 ps difference data with the theoretical models. Single product reaction models were compared with the data. The models that produce the lowest R values are then used as the initial geometries for structural refinement. For benzaldehyde, the best product fits were the models corresponding to: vibrationally “hot” ground-state benzaldehyde, benzene and carbon monoxide, benzene triplet (quinoid and anti-quinoid structures) and carbon monoxide, and benzoyl radical and atomic hydrogen. The benzene triplet is composed of equal fractions of the quinoid and anti-quinoid isomers (4.16 % each). The values of χ^2 , R , and the optimized fractions of reaction are listed in Table 7-3. The theoretical $\Delta sM(s)$ and $\Delta f(r)$ curves are compared with the data in Figs. 7-5 and 7-6. Structural refinement was attempted with each of the best models individually, and in each case a good match between theory and experiment was only possible with an unphysical structure – two long bond distances ($> 1.6 \text{ \AA}$) in the aryl ring. It was concluded that these models individually were each too near to undesired local minima and that a combination of them must be used to account for some more complicated photoreaction.

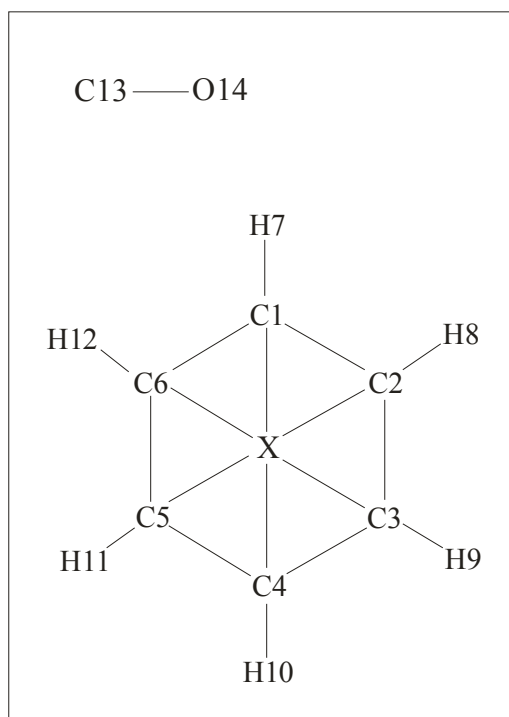
Table 7-4. The two-component fraction fits of some benzaldehyde product channels

Product #1	Product #2	Fract. #1 (%)	Fract. #2 (%)	χ^2	<i>R</i>
Hot benzaldehyde	Benzene + CO	6.11 ± 5.56	4.08 ± 7.04	3.396	0.581
	Phenyl + formyl	7.10 ± 5.50	3.62 ± 5.97	3.507	0.569
	Benzoyl + H	9.52 ± 10.93	-1.03 ± 22.02	4.072	0.666
Benzaldehyde (T ₁)	Benzene + CO	2.82 ± 4.72	8.66 ± 7.02	4.463	0.766
	Phenyl + formyl	2.27 ± 4.68	8.46 ± 5.98	5.864	0.935
	Benzene (T ₁) + CO	-1.06 ± 4.67	6.00	2.988	0.517
Benzaldehyde (T ₂)	Benzene + CO	5.28 ± 4.60	6.34 ± 7.42	2.825	0.526
	Benzoyl + H	1.01 ± 8.63	16.67 ± 22.17	4.987	0.845
	Phenyl + formyl	6.32 ± 4.79	6.61 ± 6.63	2.928	0.526
	Benzene (T ₁) + CO	-1.84 ± 4.31	7.00	2.994	0.508
Benzoyl + H	Benzene + CO	11.90 ± 11.21	5.46 ± 7.03	3.275	0.571
	Phenyl + formyl	14.31 ± 11.60	5.44 ± 6.25	3.322	0.549

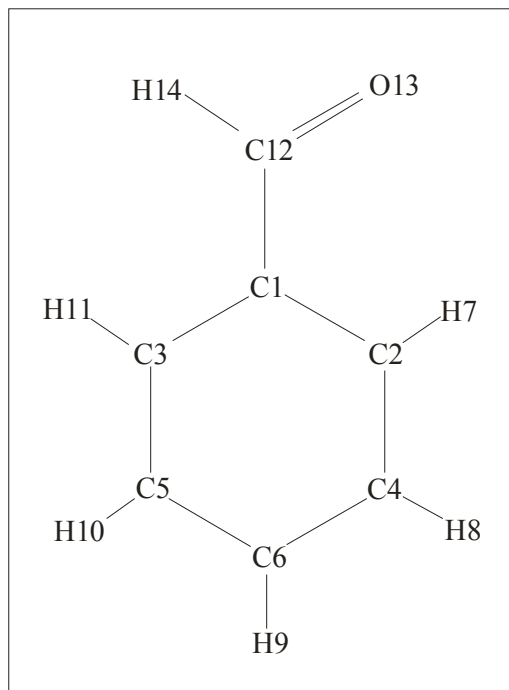
Error bars are 3 σ from the UED_2004 program.

Two-component model comparisons were then performed. Some of the two-component (just fractions and polynomial background optimized) results are listed in Table 7-4. The $\Delta sM(s)$ and $\Delta f(r)$ comparisons are displayed in Figs. 7-7, 7-8 and 7-9. It should be noted that when the products included the two isomers of triplet benzene, the fractions of the isomers could not be fit mathematically but instead had to be varied manually to locate the minimum due to a shortcoming of the fitting code in the program. Several two-product reactions can be eliminated right away since one of the products has been reduced to a fraction below zero. Structural refinements were conducted with several of the two-product models, and again, in each case two long bond distances occurred in the aryl rings. The exceptions, the good fits, were combinations where T₂ (³ $\pi\pi^*$) benzaldehyde is paired with either benzene and carbon monoxide or the phenyl and formyl radicals – also the two best matches between theory and experiment. Based on a better χ^2 and previous experimental observations of benzene and carbon monoxide as photoproducts,^{10,11,34,36-38} the molecular mixture of benzene, carbon monoxide, and triplet $\pi\pi^*$ benzaldehyde were concluded to be the products of this reaction.

X						
C1	X	r1				
C2	X	r1	C1	a1		
C3	X	r1	C2	a1	C1	d1
C4	X	r1	C3	a1	C2	d2
C5	X	r1	C4	a1	C3	d3
C6	X	r1	C5	a1	C4	d4
H7	C1	r2	C2	a2	C6	d5
H8	C2	r2	C3	a2	C1	d6
H9	C3	r2	C4	a2	C2	d7
H10	C4	r2	C5	a2	C3	d8
H11	C5	r2	C6	a2	C4	d9
H12	C6	r2	C1	a2	C5	d10
C13	C1	r3	C2	a3	C3	d11
O14	C13	r4	C1	a4	C2	d12



C1						
C2	C1	r1				
C3	C1	r1	C2	a1		
C4	C2	r2	C1	a2	C3	d1
C5	C3	r2	C1	a2	C2	d2
C6	C1	r3	C2	=a1/2	C3	d3
H7	C2	r4	C1	=180-a2/2	C4	d4
H8	C4	r5	C2	a3	C6	d5
H9	C6	r6	C1	a4	C2	d6
H10	C5	r5	C3	a3	C6	d7
H11	C3	r4	C1	=180-a2/2	C5	d8
C12	C1	r7	C3	=180-a1/2	C2	d9
O13	C12	r8	C1	a5	C2	d10
H14	C12	r9	O13	a6	C1	d11



The final refined theoretical $\Delta sM(s)$ and $\Delta f(r)$ are shown with the data in Fig. 7-10 ($\chi^2 = 2.101$; $R = 0.404$). The structural parameters are listed in Table 7-5. A C_{2v}

model was used for the quinoid benzaldehyde triplet; *ab initio* calculations predict near- C_{2v} symmetry. Since preliminary refinements were rather insensitive to the carbonyl torsional angle, it was fixed at planarity for the final refinement (as predicted by theory). The structure of the ground-state benzene product was refined with a D_{6h} model. The $C\equiv O$ distance of carbon monoxide and all structural parameters involving hydrogen atoms were fixed at *ab initio* or DFT-derived values. The temperature of the benzene and CO products was fixed at 500 K and the temperature of benzaldehyde T_2 at 1000 K, near to estimated values. Contrasting the results of the fit to the theoretically calculated structure shows few deviations. Most notably, the double bonds of the quinoid ring are somewhat shorter than their theoretical counterparts (1.322/1.322 Å vs. 1.362/1.358 Å, respectively) emphasizing the more electron-localized, $\pi\pi^*$ character. Unlike previous UED results, the structure obtained here allows for direct comparison between the theoretically and experimentally determined structures of an excited state.

Table 7-5. The refined structures of the products of benzaldehyde photolysis

Product species	Parameters	UED value ^a	Theoretical ^b
carbon monoxide	$r(\text{C-O})$	-	1.127
benzene	$r(\text{X-C})$	1.371 ± 0.004	1.393
	$r(\text{C-H})$	-	1.084
	$a(\text{C-C-C})$	-	120.0
	$a(\text{H-C-C})$	-	120.0
T_2 benzaldehyde ^c $\pi\pi^*$	$r(\text{C1-C2}), r(\text{C1-C3})$	1.479 ± 0.029	1.484, 1.471
	$r(\text{C2-C4}), r(\text{C3-C5})$	1.322 ± 0.029	1.362, 1.358
	$r(\text{C1-C6})$	2.909 ± 0.084	2.857
	$r(\text{C2-C4}), r(\text{C3-C5})$	1.487^{d}	1.442, 1.460
	$r(\text{C1-C7})$	1.420 ± 0.045	1.421
	$r(\text{C7-O8})$	1.263 ± 0.031	1.237
	$r(\text{C2-H7}), r(\text{C3-H11})$	-	1.071, 1.075
	$r(\text{C4-H8}), r(\text{C5-H10})$	-	1.075, 1.074
	$r(\text{C6-H9})$	-	1.072
	$r(\text{C12-H14})$	-	1.088
	$a(\text{C2-C1-C3})$	115.6 ± 6.2	117.8
	$a(\text{C1-C2-C4}), a(\text{C1-C3-C5})$	122.3 ± 7.7	120.3, 120.7
	$a(\text{C2-C4-C6}), a(\text{C3-C5-C6})$	122.4^{d}	121.2, 120.8
	$a(\text{C4-C6-C5})$	115.0^{d}	119.2
	$a(\text{C3-C1-C12})$	122.2^{d}	121.3
	$a(\text{C1-C12-O13})$	125.4 ± 2.6	123.1
	$a(\text{H7-C2-C1}), a(\text{H11-C3-C1})$	118.9^{d}	117.9, 118.5
	$a(\text{C8-C4-C2}), a(\text{C10-C5-C3})$	-	119.9, 120.2
	$a(\text{C9-C6-C1})$	-	180.0
	$a(\text{H14-C12-O13})$	-	119.2
$d(\text{C2-C1-C12-O13})$	-	0.0	

a) The error bars reported here are 3σ from the Uedana program.

b) Theoretical structures were obtained at B3LYP/6-311G(d,p) for benzene, carbon monoxide, methyl, and benzoyl. CASSCF(9,10)/6-31G(d) was used for the excited state (T_2) of benzaldehyde.

c) C_{2v} symmetry was imposed for the phenyl ring.

d) Dependent variables.

With the product structures determined, their contribution at each of the time points is evaluated via linear parameter fitting of the fractions and polynomial background terms. Fig. 7-11 shows the time-resolved theoretical and experimental $\Delta sM(s)$ and $\Delta f(r)$ curves at each of the time points using the refined products structures to calculate the theoretical $\Delta sM(s)$. The experimentally determined population change with time is shown in Fig. 7-12; relative product fractions at each time point are listed in Table 7-6.

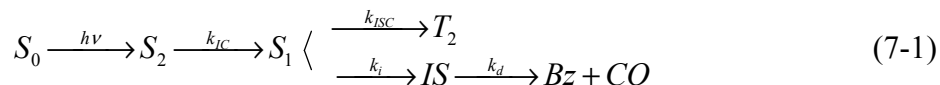
Table 7-6. The fractional contributions of the product molecules at each time point.

Time (ps)	Fraction (%)			
	T ₂ benzaldehyde	benzene + CO	χ^2	<i>R</i>
-100	0	0	-	-
-50	0	0	-	-
-10	0	0	-	-
-5	1.7 ± 3.6	0.6 ± 4.3	2.747	3.063
0	3.5 ± 3.2	0.9 ± 4.5	3.411	1.684
5	5.3 ± 3.1	2.3 ± 4.4	3.583	1.069
10	5.6 ± 3.7	2.1 ± 4.4	2.625	0.877
15	5.1 ± 3.6	2.4 ± 4.3	2.768	0.940
20	7.4 ± 3.5	3.4 ± 4.2	2.853	0.667
30	7.3 ± 3.6	4.3 ± 4.3	2.694	0.596
40	8.2 ± 3.7	5.4 ± 4.4	2.577	0.493
50	9.1 ± 3.3	5.9 ± 4.1	2.100	0.405
100	9.0 ± 3.7	6.7 ± 4.3	3.767	0.516
1000	10.9 ± 3.3	6.7 ± 4.6	3.282	0.431

The error bars (3 σ from Uedana) have the weight factor removed (see Section 4.4.1).

Both the photophysical (T₂, $\pi\pi^*$ benzaldehyde) and photochemical (benzene + CO) channels products grow simultaneously. The apparent rise time constant of the channel forming T₂ benzaldehyde is 25 ± 4 ps, determined by nonlinear fitting of a single step reaction (see Section 4.6). The rise time constant of the benzene-forming channel is somewhat longer, 38 ± 5 ps. The final percent populations of T₂ benzaldehyde and benzene are $10.9 \pm 3.3\%$ and $6.7 \pm 4.6\%$, respectively, after reaching stationary state; the percentage is in reference to the total population of all species (including the parent that was subtracted out when constructing the difference data). The nearly parallel behavior of the two-product channels implies competitive bifurcation after origination from a single state, as no growth of one at the expense of the other was observed. At the excitation used (266.7 nm), it is known that the $\pi\pi^*$ S₂ state has an ultrashort lifetime (~ 250 fs¹⁹). Because of this, and the fact that ISC is more efficient between states of different orbital excitations ($\pi\pi^*/n\pi^*$), it follows that T₂ ($\pi\pi^*$) benzaldehyde must form from an $n\pi^*$ state via an efficient ISC, making S₁ benzaldehyde the origin state of bifurcation.

The bifurcation model of benzaldehyde can now be written as follows:



An intermediate structure (*IS*) is included in order to account for the difference in the rise time of the two channels bifurcated from the hot S_1 $n\pi^*$ state. The presence of the *IS* is further supported by the electronic nature of S_1 – dissociation from the $n\pi^*$ excited state correlates with the electronically excited state of CO, which is not seen in the data. It follows that the total decay rate of the S_1 population is given by

$$k = k_{ISC} + k_i \quad (7-2)$$

and the product branching ratio is

$$\frac{P(T_2)}{P(Bz + CO)} = \frac{k_{ISC}}{k_i}. \quad (7-3)$$

From the rise time of 25 ± 4 ps ($k = 4.0 \times 10^{10} \pm 0.6 \times 10^{10} \text{ s}^{-1}$) for the faster channel and a branching ratio ($T_2 : Bz + CO$) of $10.9 \pm 3.3\% : 6.7 \pm 4.6\%$, the rate constants are found to be $k_{ISC} = 2.4 \times 10^{10} \text{ s}^{-1}$ ($1/k_{ISC} = 42$ ps) and $k_i = 1.6 \times 10^{10} \text{ s}^{-1}$ ($1/k_i = 61$ ps). A simulation of the population changes based on this bifurcation model is shown with the data in Fig. 7-12; k_d was taken to be $9.4 \times 10^{10} \text{ s}^{-1}$ ($1/k_d = 11$ ps) from the initial rise of the benzene channel. The decay of the S_1 was not seen due to its structural similarity with the parent S_0 ; the very short-lived *IS* structure was not detectable because of its small population (see Fig. 7-13).

7.3.2. The time-resolved structures of acetophenone

Diffraction data at three time points (−100 ps, +50 ps, and +100 ps) were taken for acetophenone. The full temporal range of experimentation was limited because of inlet window coating as mentioned in Section 7.2. The data from −100 ps were used as the reference and subtracted from the two positive time points to generate the difference data. The difference images are shown in Fig. 7-13 and the corresponding one-dimensional difference curves [$R^N(\text{pix})$ in Eq. (4-9)] are shown in Fig. 7-14. Perusal of both patterns and curves reveals a signal that is nearly, but not entirely, saturated 50 ps after the excitation laser pulse. Product analysis was conducted on both time points and found to yield nearly equivalent results. The results presented hereafter were arrived at through analysis of the +50 ps difference data, unless otherwise noted.

Table 7-7. The fraction fits of some acetophenone product channels

Product	Fraction (%)	χ^2	R
Hot acetophenone (2500 K)	15.04 ± 5.80	8.714	0.717
Toluene + CO	14.53 ± 7.31	7.643	0.636
Phenyl + acetyl radicals	11.08 ± 4.99	13.499	1.084
Benzoyl + methyl radicals	18.10 ± 8.26	13.806	1.107
Toluene (T ₁) + CO	9.27 ± 4.91	8.990	0.699
Acetophenone T ₁	−11.12 ± 5.38	19.195	1.499
Acetophenone S ₁	−10.38 ± 5.08	19.423	1.567
Acetophenone T ₂	10.42 ± 4.69	17.960	1.590

Error bars are 3σ from UED_2004.

Determination of the products of acetophenone photolysis was performed similar to that described previously for benzaldehyde. First, structures proposed in the literature and those predicted by calculations (Fig. 7-15) were compared with the difference data. Products used in these comparisons have mostly been speculated by previous photochemical and photophysical work. The optimized fractions of each possible channel (acetophenone at 503 K is the parent molecule) are listed in Table 7-7 and the

$\Delta sM(s)$ and $\Delta f(r)$ curves are shown in Figs. 7-16 and 7-17. The product temperatures were roughly estimated from the available energy after 266.7 nm excitation of S_0 acetophenone. The internal microcanonical temperature assuming internal conversion back to S_0 was taken to be 2500 K; the temperatures of other pathways were set at 700 K. The best single-product fit is the channel leading to toluene and carbon monoxide as products. Attempts at structural refinement of the toluene as a product caused separation of the methyl group from the aromatic ring and lengthening of aromatic bonds to $> 1.6 \text{ \AA}$ – a highly unphysical structure and clear evidence that the product is something else. Similar results were had with other single product test refinements, a sign that perhaps the decay of excited acetophenone forms multiple structures. Reactions producing two product structures were then tested with the data – the optimized fractions and χ^2 and R values are listed in Table 7-8, and the $\Delta sM(s)$ and $\Delta f(r)$ curves are shown in Figs. 7-18, 7-19, and 7-20. Some combinations can be immediately excluded as candidates since the optimized fraction of one product either becomes negligible (less than the error bar) or becomes less than zero. Structural refinements were conducted on some of the best of the remaining possible combinations.

Table 7-8. The two-component fraction fits of some acetophenone product channels

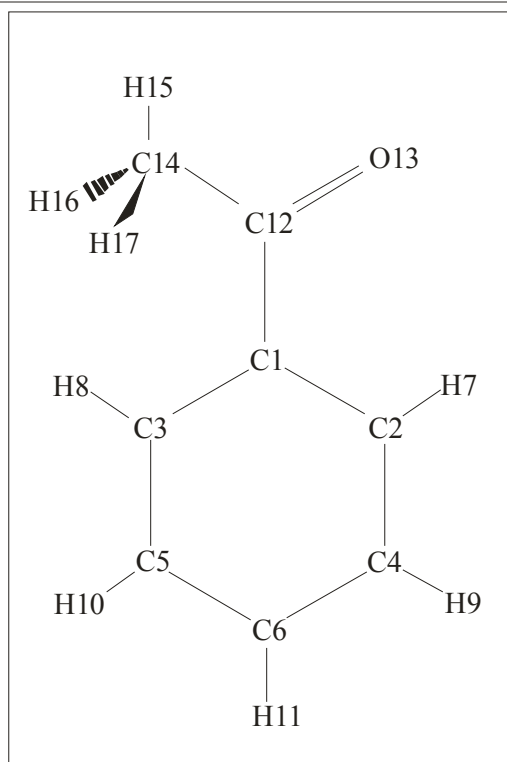
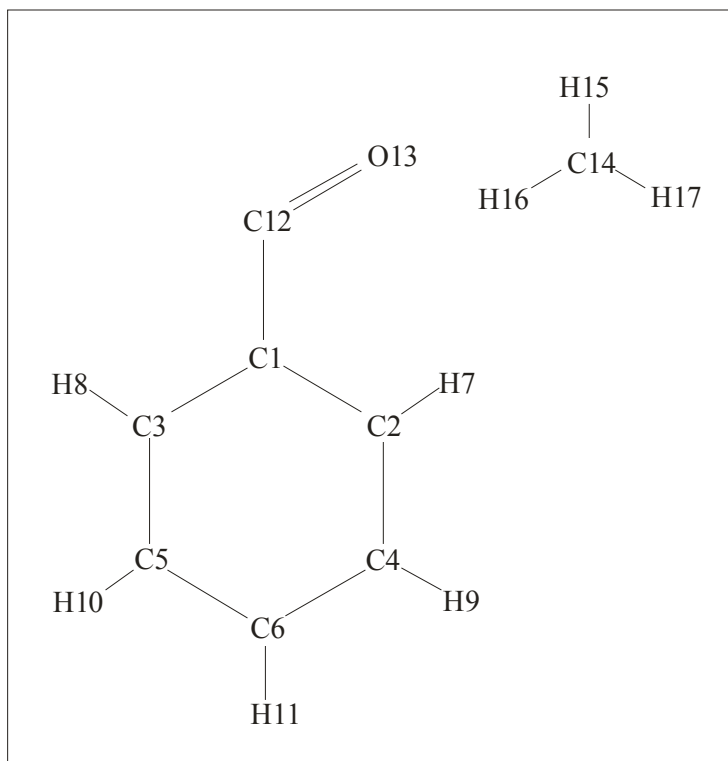
Product #1	Product #2	Fract. #1 (%)	Fract. #2 (%)	χ^2	R
Hot acetophenone	Benzoyl + methyl	11.78 ± 5.82	9.04 ± 8.29	6.774	0.600
	Phenyl + acetyl	12.49 ± 6.23	3.10 ± 5.36	8.302	0.693
	Toluene + CO	7.00 ± 6.69	9.16 ± 8.43	6.525	0.584
Acetophenone (T_1)	Phenyl + acetyl	-7.06 ± 5.40	9.65 ± 5.00	11.513	0.869
	Toluene + CO	-3.98 ± 5.38	13.38 ± 7.31	7.062	0.590
	Toluene (T) + CO	-6.02 ± 5.54	8.40 ± 5.05	7.553	0.580
Acetophenone (T_2)	Benzoyl + methyl	9.99 ± 5.81	17.64 ± 10.23	7.746	0.646
	Phenyl + acetyl	9.54 ± 5.53	10.54 ± 5.88	7.990	0.667
	Toluene (T) + CO	-4.83 ± 7.83	11.44 ± 8.20	8.419	0.661
	Toluene + CO	4.11 ± 4.69	13.03 ± 7.31	6.797	0.584
Benzoyl + methyl	Phenyl + acetyl	8.96 ± 11.14	6.47 ± 6.72	12.780	1.020
Toluene + CO	Toluene (T) + CO	9.62 ± 7.73	3.87 ± 5.20	6.863	0.583

Error bars are 3σ from UED_2004.

The molecular dissociation pathway coupled with intersystem crossing to T_2 , which had worked well for benzaldehyde, was not compatible with the acetophenone data despite the favorable *ab initio* comparison. Refinement of that model caused the contribution of T_2 acetophenone to be eliminated entirely leaving only toluene and carbon monoxide. The structure of toluene was also changed significantly; two of the C–C bonds of the aryl ring stretched to 1.57 Å and the methyl group became separated from the ring by 1.98 Å. The improbable geometry excluded this product channel from further consideration. Also worthy of consideration were the possible reactions yielding vibrationally excited S_0 acetophenone and either the benzoyl and methyl radicals or toluene and carbon monoxide. Both models also became unphysical with structural refinement. The acetyl group separated from S_0 acetophenone and long bond distances stretched the aromatic rings. It's a perfect example of how diffraction data may have multiple solutions and it is up to us as chemists to use our knowledge and intuition to determine which solution is the correct one. In the case of acetophenone, the model

refining to physical structures was the one that represented the channel forming T₂ acetophenone and the benzoyl and methyl radicals.

C1						
C2	C1	r1				
C3	C1	r1	C2	a1		
C4	C2	r1-0.011	C1	a1-0.5	C3	d1
C5	C3	r1-0.011	C1	a1-0.5	C2	d2
C6	C1	r2	C2	a1/2	C3	d3
H7	C2	r3	C1	180-a1/2	C4	d4
H8	C3	r3	C1	180-a1/2	C5	d5
H9	C4	r4	C2	a2	C6	d6
H10	C5	r4	C3	a2	C6	d7
H11	C6	r5	C1	a3	C2	d8
C12	C1	r6	C3	180-a1/2	C2	d9
O13	C12	r7	C1	a4	C2	d10
C14	C12	r8	O13	180-a4/2	C1	d11
H15	C14	r9	C12	a5	O13	d12
H16	C14	r10	H15	a6	C12	d13
H17	C14	r11	H16	a7	H15	d14



C1						
C2	C1	r1				
C3	C1	r1	C2	a1		
C4	C2	r2	C1	a1+3.35	C3	d1
C5	C3	r2	C1	a1+3.35	C2	d2
C6	C1	r3	C2	a1/2	C3	d3
H7	C2	r4	C1	178.325-a1/2	C4	d4
H8	C3	r4	C1	178.325-a1/2	C5	d5
H9	C4	r5	C2	a2	C6	d6
H10	C5	r5	C3	a2	C6	d7
H11	C6	r6	C1	a3	C2	d8
C12	C1	r1-0.0345	C3	180-a1/2	C2	d9
O13	C12	r7	C1	a4	C2	d10
C14	C12	r1+0.0355	O13	180-a4/2	C1	d11
H15	C14	r8	C12	a5	O13	d12
H16	C14	r9	C12	a6	H15	d13
H17	C14	r10	C12	a7	H15	d14

Well-behaved structural refinement was found with this model. Several constraints had to be added to the z-matrices since so many parameters needed to be refined (see below). The final refined theoretical and experimental $\Delta sM(s)$ and $\Delta f(r)$ curves are shown in Fig. 7-21. The oscillations in $\Delta f(r)$ at longer distances were never matched exactly, regardless of the model used, and must have been due to some unknown factor. The negative peaks at ~ 1.5 and ~ 2.5 Å correspond to the loss of internuclear distances and are evidence of the fragmentation that occurs. The fitted structural parameters are listed in Table 7-9 along with those predicted by theory. In this refinement

it was necessary to employ structural dependencies to simplify the fitting. In addition to the restriction of C_{2v} symmetry for the aryl rings in both benzoyl radical and T_2 acetophenone, the models of both molecules were further restricted. Only one distance and one angle were refined in the ring of the benzoyl radical and, for T_2 acetophenone, all single bonds were defined by one “fittable” parameter. Furthermore, the skeletal angles of the T_2 acetophenone ring were defined as one, as were the angles of the carbonyl moiety. And, as is typical of all ring structures, some parameters were unable to be defined and simply drifted with the changes of the other, “fittable” parameters. The torsional angles for carbonyl groups in the benzoyl radical and in T_2 acetophenone were fixed in the plane of the ring as indicated by theory and preliminary fitting results. Differences between the parameters derived from the diffraction data and those calculated by theory were less than 0.03 Å for direct bond distances and 3 ° for angles, or were within the error bar. The double and single bonds of the T_2 acetophenone ring are clearly resolved demonstrating the loss of aromaticity and its $\pi\pi^*$ nature. The theory matches experiment with $\chi^2 = 4.841$ and $R = 0.473$.

Table 7-9. The refined structures of acetophenone photolysis products.

Species	Parameters	UED value ^a	theoretical ^b
Methyl radical	$r(\text{C-H})$	-	1.080
	$a(\text{H-C-H})$	-	120.0
Benzoyl radical	$r(\text{C1-C2}), r(\text{C-C3})$	1.403 ± 0.024	1.403, 1.398
	$r(\text{C2-C4}), r(\text{C3-C5})$	1.392 ^d	1.388, 1.391
	$r(\text{C1-C6})$	2.700 ± 0.033	2.781
	$r(\text{C4-C6}), r(\text{C5-C6})$	1.370 ^d	1.397, 1.394
	$r(\text{C1-C12})$	1.487 ± 0.032	1.482
	$r(\text{C12-O13})$	1.164 ± 0.009	1.186
	$r(\text{C2-H7}), r(\text{C3-H8})$	-	1.084, 1.084
	$r(\text{C4-H9}), r(\text{C5-H10})$	-	1.084, 1.084
	$r(\text{C6-H11})$	-	1.084
	$a(\text{C2-C1-C3})$	120.6 ± 1.1	120.2
	$a(\text{C1-C2-C4}), a(\text{C1-C3-C5})$	120.1 ^d	119.7, 119.9
	$a(\text{C2-C4-C6}), a(\text{C3-C5-C6})$	116.2 ^d	119.9, 119.8
	$a(\text{C4-C6-C5})$	127.0 ^d	120.5
	$a(\text{C2-C1-C12})$	119.7 ^d	120.5
	$a(\text{C1-C12-O13})$	130.6 ± 2.7	128.5
	$a(\text{H7-C2-C1}), a(\text{H8-C3-C1})$	119.7 ^d	119.0, 119.0
	$a(\text{H9-C4-C2}), a(\text{H10-C5-C3})$	-	120.0, 120.1
	$a(\text{H11-C6-C1})$	-	180.0
	$d(\text{C2-C1-C12-O13})$	-	0.0
	T ₂ acetophenone ^c	$r(\text{C1-C2}), r(\text{C1-C3})$	1.495 ± 0.014
$r(\text{C2-C4}), r(\text{C3-C5})$		1.349 ± 0.021	1.358, 1.356
$r(\text{C1-C6})$		2.827 ± 0.065	2.866
$r(\text{C4-C6}), r(\text{C5-C6})$		1.441 ^d	1.446, 1.462
$r(\text{C1-C12})$		1.460 ^d	1.446
$r(\text{C12-O13})$		1.214 ± 0.018	1.224
$r(\text{C12-C14})$		1.530 ^d	1.516
$r(\text{C2-H7}), r(\text{C3-H8})$		-	1.071, 1.073
$r(\text{C4-H9}), r(\text{C5-H10})$		-	1.075, 1.075
$r(\text{C6-H11})$		-	1.071
$r(\text{C14-H15})$		-	1.081
$r(\text{C14-H16}), r(\text{C14-H17})$		-	1.086, 1.086
$a(\text{C2-C1-C3})$		117.3 ± 1.3	117.4
$a(\text{C1-C2-C4}), a(\text{C1-C3-C5})$		120.7 ^d	120.7, 120.8
$a(\text{C2-C4-C6}), a(\text{C3-C5-C6})$		119.7 ^d	121.1, 121.1
$a(\text{C4-C6-C5})$		121.9 ^d	118.8
$a(\text{C2-C1-C12})$		121.3 ^d	119.2
$a(\text{C1-C12-O13})$		126.0 ± 7.9	119.8
$a(\text{C13-C12-C14})$		117.0 ^d	120.4
$a(\text{H7-C2-C1}), a(\text{H8-C3-C1})$		119.7 ^d	117.0, 119.3
$a(\text{H9-C4-C2}), a(\text{H10-C5-C3})$		-	120.0, 120.1
$a(\text{H11-C6-C1})$		-	180.0
$a(\text{H15-C14-C12})$		-	108.5
$a(\text{H16-C14-C12}), a(\text{H17-C14-C12})$	-	111.2, 111.2	
$d(\text{C2-C1-C12-O13})$	-	0.0	
$d(\text{H15-C14-C12-O13})$	-	0.0	

a) The error bars reported here are 3σ from Uedana.

b) Theoretical structures were obtained at B3LYP/6-311G(d,p) for methyl and benzoyl. CASSCF(9,10)/6-311G(d,p) was used for the excited state (T₂) of acetophenone.

- c) C_{2v} symmetry was imposed for the phenyl ring.
 d) Dependent variables.

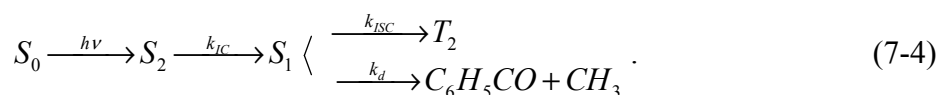
Upon the determination of the structures of the reaction products, their fractional contributions were obtained at the +100 ps difference data time point (recall that structural refinement was conducted at the +50 ps difference time point). From +50 to +100 ps the fractional amount of T_2 acetophenone remains unchanged, but the amount of fragmentation into benzoyl and methyl radicals increases over the two time points as displayed in Table 7-10.

Table 7-10. Relative product compositions.

Time delay (ps)	Products fractions (%)			
	T_2 acetophenone	benzoyl + methyl radicals	χ^2	R
-100	0	0	-	-
50	8.9 ± 4.6	11.9 ± 4.7	4.842	0.474
100	8.4 ± 4.6	16.8 ± 4.6	4.776	0.400

a) The error bars reported here are 3σ .

This is a similar case to that reported above for benzaldehyde where dissociation also occurs at a slower rate. Because of the limited data points, the exact nature of the bifurcation cannot be elucidated, however, the structures determined lead, in analogy with benzaldehyde, to the following mechanism:



The relative fractions of the products are listed in Table 7-10. The observed structures involved in the photophysical and photochemical bifurcations in both benzaldehyde and acetophenone are shown schematically in Fig. 7-22.

7.4. Discussion of results

The results of the UED studies of benzaldehyde and acetophenone can be summarized as follows: The structural changes of both molecules were studied following ultrafast laser excitation at 266.7 nm to the S_2 ($\pi\pi^*$) excited state. The photophysical and photochemical channels were observed in competition and the resultant molecular structures characterized. Time scales were also determined.

The structures present in the time-resolved diffraction data for acetophenone and benzaldehyde result from the bifurcation on the excited S_1 $n\pi^*$ state, following femtosecond internal conversion from S_2 , which results in the formation of a quinoid triplet structure and the products of dissociation. For benzaldehyde the dissociation products are the closed-shell molecular species, benzene and carbon monoxide. For acetophenone they are the benzoyl and methyl radicals.

7.4.1. Structural dynamics

Given the UED results above, the following dynamical picture of aromatic carbonyl photophysics and photochemistry can be drawn. Excitation at 266.7 nm promotes population of both acetophenone and benzaldehyde into the $\pi\pi^*$ S_2 state, which decays rapidly by internal conversion into S_1 . For benzaldehyde at 266.7 nm excitation, the decay time is roughly 250 fs and for acetophenone S_2 lives less than 140 fs.¹⁹ In the nascent vibrational levels of S_1 , aromatic carbonyl molecules experience a bifurcation of pathways. A physical pathway moves some population into the triplet manifold, the $\pi\pi^*$ T_2 state, and a competitive chemical pathway causes dissociation into products.

For benzaldehyde, the physical channel (ISC) from S_1 proceeds with a rate of $2.4 \times 10^{10} \text{ s}^{-1}$ ($1/k_{ISC} = 42 \text{ ps}$), and survives up to at least 1 ns; the measured rate is $k_{ISC} + k_i$ [see Eq. (7-2)]. The triplet structure was identified as that of the $\pi\pi^*$ T_2 and, compared to the ground state, the phenyl ring is seen to distort as aromaticity is lost – two double bonds and four single bonds make up the quinoid ring. Along the chemical pathway, the benzene and carbon monoxide products are formed stepwise, involving an intermediate state, IS , as determined by the observed kinetics detailed in Section 7.4.2.

After internal conversion to the $\pi\pi^*$ S_1 , excitation is localized mainly on the C=O bond of the carbonyl group. According to quantum chemical calculations, the carbonyl group remains coplanar with the phenyl ring, however, the H–C=O out-of-plane bending mode is reduced in frequency (642 cm^{-1} on $\pi\pi^*$ compared with 1033 cm^{-1} on S_0). The more facile large-amplitude motion of the aldehydic hydrogen atom allows for its capture by C1 and the subsequent formation of a transition state (TS) where the H is shared by C1 and C12 (shown in Fig. 7-23). This TS connects the $\pi\pi^*$ state to IS where C1 is sp^3 hybridized and bound to both H and CO (also shown in Fig. 7-23). The aldehydic hydrogen atom and the CO moiety are loosely bound and distorted from the molecular plane and either one can be lost from IS by simple cleavage. Perturbation present in the C=O moiety of the $\pi\pi^*$ state switches in the intermediate to a $\pi\pi^*$ -like perturbation of the phenyl group resulting in a “pseudo-fulvenic” six-membered ring structure. The C=O distance in the intermediate is identical to the C=O distance of the acetyl radical ground state (1.180 Å), indicating the stability of the CO moiety.

Table 7-11. Statistical and mode-limited rate constants.

System	Channel	Energy ^{a,b} (cm ⁻¹)				Rate ^{c,d} (s ⁻¹)			
		Reactant	TS	IS	Product	k ₆	k _n	k _s	
benzaldehyde	S ₀	- CO	0	32218	-	460	1.7×10 ¹⁰	2.1×10 ⁸	5.4×10 ⁰
		- H	0	-	-	32679			
		- C ₆ H ₅	0	-	-	34611			
	S ₁	- CO	26921	35474	28439	30087	1.6×10 ¹¹	1.3×10 ¹⁰	1.0×10 ⁷
		- H	26921	36297	-	32682	7.7×10 ¹⁰	5.6×10 ⁹	6.6×10 ⁶
		- C ₆ H ₅	26921	36772	-	34611	5.0×10 ¹⁰	3.9×10 ⁹	1.6×10 ⁷
acetophenone	S ₀	- CO	0	33697	-	1816	6.2×10 ⁹	1.4×10 ⁵	8.0×10 ⁻³
		- CH ₃	0	-	-	29751			
		- C ₆ H ₅	0	-	-	34291			
	S ₁	- CO	27279	×	29810	30890			
		- CH ₃	27279	34257	-	29751	6.7×10 ¹¹	1.6×10 ¹⁰	3.5×10 ⁸
		- C ₆ H ₅	27279	36951	-	34291	3.5×10 ¹⁰	2.1×10 ⁸	2.9×10 ⁶

a) Energy corrections for S₁ (nπ*) reactions are 3906 and 3710 cm⁻¹ for benzaldehyde and acetophenone, respectively. (see Section 7.2)

b) Energy corrections for products are 2276 cm⁻¹ for C₆H₅CO + H and 3091 cm⁻¹ for C₆H₅CO + CH₃.

a) k₆, k_n, and k_s denote statistical rate constants for various models of energy coupling among phenyl, methyl, and carbonyl groups. k₆ (for six involved modes) is obtained by assuming that the phenyl and methyl groups do not participate in energy randomization (spectator model), and k_s by assuming full randomization of reactant energy amongst all vibrational modes. k_n is obtained by assuming partial randomization where only *n* vibrational modes participate in the dissociation; *n* = 10 for benzaldehyde and *n* = 16 for acetophenone are used.

d). Thermal energies at 500 K were added to the excitation energy of 37500 cm⁻¹ (266.7 nm).

UED results show that the rearrangement step (S₁ to *IS*) takes place at a rate of 1.6×10¹⁰ s⁻¹ (1/k_i = 61 ps) ; the measured rate is k_{ISC} + k_i [see Eq. (7-2)]. But, statistical Rice-Ramsperger-Kassel-Marcus (RRKM)⁶⁰ calculations predict a rate several orders of magnitude slower (see Table 7-11), implying that energy redistribution among vibrational modes may be incomplete. The TS between the nπ* state and *IS* is lower in energy than both the nπ* TS leading to benzoyl and hydrogen radicals as well as an S₀ TS leading directly to benzene and carbon monoxide products. The structures of the various theoretical transition states and intermediates are shown in Fig. 7-23. Passage from the excited state *IS* to the products may proceed in different ways. The most direct route would be dissociation of CO from *IS*. However, an alternative route exists through the

ground state – although a frequency calculation confirms the stability of *IS* in the excited state, it immediately undergoes CO loss when put on the S_0 surface. Internal conversion of *IS* followed by instantaneous dissociation could be the more likely path. The threshold energy for benzene formation from benzaldehyde is known to be just below the S_2 origin with which the above theoretical estimation agrees quite reasonably.^{4,6,11,15} If instead one were to assume that the molecular dissociation occurs after internal conversion from S_1 to S_0 , the calculations indicate that the large barrier height (32218 cm^{-1}) will render the reaction much slower than the time scale observed (see Table 7-11).

For acetophenone, the bifurcation from S_1 is also seen as a competition between chemical and physical pathways. The physical pathway results in the formation of a $\pi\pi^*$ triplet, structurally similar to the quinoid-like system seen for benzaldehyde (with the additional methyl group, of course). However, the chemical result is quite different. On the excited state surface, the methyl group does not show the same propensity for large-amplitude motion as was seen for the aldehydic hydrogen of S_1 benzaldehyde and its capture by the phenyl ring does not occur. In other words, a pathway (or TS) could not be found for the molecular dissociation channel from the $\pi\pi^*$ state – although an *IS* structure like that found for the benzaldehyde dissociation can be calculated for acetophenone (see Fig. 7-23), no direct trajectory exists to link it to S_1 . Methyl loss is the lowest energy chemical channel found from the $\pi\pi^*$ surface. The quantum chemical calculations above agree well with the experimental observations; molecular dissociation for benzaldehyde and radical cleavage for acetophenone are the favored chemical pathways from their respective $\pi\pi^*$ states.

7.4.2. The UED results in context

The T_2 states of acetophenone and benzaldehyde are electronic states that have eluded direct characterization by all previous experimental methods. As described in Section 7.1, phosphorescence studies have supplied all that is known of the state and its relationship to the bright T_1 . Some previous researchers^{10,37} employed a kinetic model with an intermediate state in the triplet manifold, possessing a lifetime long enough to explain the collision-induced quenching of chemistry and the enhancement of phosphorescence in high-pressure environments. The UED results permit us to identify this reactive, yet quenchable, intermediate as T_2 . If T_2 is allowed to evolve in the absence of collisions, dissociation occurs to produce the triplet benzene observed by other researchers on longer time scales.^{37,38} The dissociation time constant for this reaction would be about 80 ns at 266.7 nm excitation energy. The triplet state of benzene ($\pi\pi^*$) and ground state of CO theoretically correlate as molecular dissociation products of T_2 $\pi\pi^*$ benzaldehyde. If, however, T_2 loses its excess vibrational energy through collisions, the only significant relaxation pathway becomes phosphorescent emission through T_1 . In other words, phosphorescence is the dominant process in aromatic carbonyl compounds possessing little excess energy above the S_1 origin. In the isolated molecule, at energies above S_2 excitation the expected yield of benzene and carbon monoxide is nearly unity (phosphorescence is a minor channel).^{3,10,36} This unity yield of benzene is actually the sum of two separate benzene-forming reactions: the fast singlet channel and the slow triplet channel.

The steady population of T_2 up to 1 ns delay seen by UED confirms the slowness of a further chemical channel but also signifies the lack of irreversible population transfer to T_1 . Since the energy gap between T_2 and T_1 is known to be so small, it may be explained by a mixed state or by rapid and “reversible” internal conversion between the two. However, the structural similarity of T_1 and S_0 precludes the detection of T_1 in this UED study, and confirmation of its presence was not possible.

Benzene formation through the photodissociation of benzaldehyde has previously been the subject of multi-photon ionization (MPI) studies using different pulse widths.^{34-36,38} These inquiries have provided a reaction time scale between 20 ps and 2 ns. In order to unite the UED results with these from the literature, simulations of population evolution have been performed following the photophysical and photochemical mechanism described in Eq. (7-1) and using the rate constants available. Population changes were calculated by numerical integration of the differential equations of the kinetic model using the fourth-order Runge-Kutta method.⁶¹ Multi-photon ionization of neutral species to their ionic counterparts were also included. Laser pulse widths of 110 fs, 20 ps, and 2 ns are used to model each type of experiment (ours and others, see Refs. 34, 35, and 36). The time-dependent population changes and laser profiles are shown in Fig. 7-24. Using a 20 ps ultraviolet pulse, the simulation predicts a branching ratio of 94% : 6% for molecular and benzene ion yields, respectively, while one for a 2 ns excitation laser pulse predicts a ratio of 6% : 94%. Both results are in qualitative agreement with the MPI experiments.³⁴ It should be noted that the simulation is based on the assumption that two-photon absorption cross-sections for photoionizations of both

excited benzaldehyde and ground state benzene are similar, although in reality they should strongly depend on wavelength, electronic structure, and resonance.

To understand the differences between the photochemistry of acetophenone and benzaldehyde better, it is valuable to compare them with the aliphatic carbonyl molecules acetone and acetaldehyde (refer to Fig. 7-25). Acetaldehyde is a prototypical aldehyde and is known to undergo molecular dissociation (CO abstraction)⁶²⁻⁶⁴ as well as homolytic cleavage (radical fragmentation) upon UV absorption. The radical channel is seen to dominate the photochemistry at lower excitations while the molecular channel becomes a competitive pathway at higher energies. For acetaldehyde, the following branching ratio of the dissociation channels (molecular/radical) has been reported: 0.001 at 313.0 nm, 0.15 at 280.4 nm, 0.28 at 265.4 nm, 0.66 at 253.7 nm, and almost unity at 248.7 nm.^{62,64} For formaldehyde, between 80 and 86 kcal/mol excitation (S_1) only the formation of the hydrogen by the molecular channel is observed, above 86 kcal/mol the radical channel turns on and competes.⁶⁵ Acetone, the prototypical ketone, however, undergoes only a homolytic radical cleavage well-known as the Norrish Type-I reaction.^{59,66,67} A molecular dissociation channel has never been reported. It has been established that the molecular dissociation pathway of acetaldehyde occurs after internal conversion to the hot S_0 while radical channels take place after ISC. Radical channels via simple cleavage are possible from both the S_0 and T_1 surfaces with very different barriers, e.g., methyl loss from acetaldehyde has a barrier of 29432 cm^{-1} on S_0 and only 4410 cm^{-1} on T_1 . In acetone, which lacks a molecular dissociation pathway, the fragmentation has been attributed to reaction on the T_1 surface as determined by the measured product

energy partitioning and the time scales.^{59,67} Radical cleavage of acetone is also believed to occur after ISC to the triplet manifold, however, it has been recently proposed⁵⁹ and confirmed⁶⁸ that fragmentation may occur directly from S_1 yielding an electronically excited acetyl radical, which then undergoes internal conversion.

Based on the abovementioned theoretical results, a mechanism for the molecular dissociation channel in the aliphatic aldehydes has been proposed to begin with internal conversion from S_1 to S_0 after excitation, while the radical channel occurs after intersystem crossing moves the population from S_1 to T_1 .⁶⁴ The branching ratio of the photophysical bifurcation (internal conversion or intersystem crossing from S_1) determines the products' fractional composition (listed above). Channel switching occurs with increasing excitation energy when a surge in the density of states of S_0 increases the IC rate while the ISC rate remains virtually the same.^{62,69} It follows in acetone as well, that the physical channels dictate the chemical products resulting in complete radical cleavage.

Although there are some analogies between aromatic and aliphatic carbonyl compounds, the physics and chemistry of aromatic carbonyl molecules are more complex due to the addition of close-lying $\pi\pi^*$ states to the manifold of low-lying $n\pi^*$ states provided by the carbonyl group. Namely, an $n\pi^*$ state, when located near a $\pi\pi^*$ state, can provide additional pathways for an aromatic carbonyl via energetically stable intermediates. Therefore, benzaldehyde (aromatic) may perform the molecular dissociation reaction through an intermediate structure on the excited state where it is the most energetically favored channel, while acetaldehyde (aliphatic) undergoes molecular

dissociation on its ground state. Acetophenone, lacking a mobile hydrogen atom, may very well fragment following the mechanism of its aliphatic analog acetone.

7.5 Summary

Structural dynamics of the aromatic carbonyls benzaldehyde and acetophenone (see Fig. 7-26) have been studied using the methodology of ultrafast electron diffraction. Following S_2 ($\pi\pi^*$) excitation at 266.7 nm, a bifurcation of pathways between photophysics (intersystem crossing) and photochemistry (molecular dissociation or radical cleavage) was observed. Intersystem crossing in both molecules results in a “quinoid-like” structure for the excited state, T_2 ($\pi\pi^*$). The product structures revealed different chemical channels for benzaldehyde and acetophenone, elucidating the fundamental disparity between aromatic aldehydes and ketones. Theoretical calculations support that the distinction results from a more facile large-amplitude motion of the aldehydic hydrogen compared to the methyl substituent. The photophysics of these molecules is made clear as UED has allowed for the direct detection and structural characterization of the dark structure of the T_2 state. Furthermore, the relationship between physical and chemical pathways in these molecules has been elucidated and a comprehensive picture of the structure of excited-state landscapes and pathways has been drawn.

7.6 References

- ¹ R. Srinivasan, J. S. Feenstra, S. T. Park, S. Xu, and A. H. Zewail, *Science* 307, 558 (2005); J. S. Feenstra, S. T. Park, and A. H. Zewail, *J. Chem. Phys.* 123, 221104 (2005); S. T. Park, J. S. Feenstra, and Z. A.H., *J. Chem. Phys.* 124, 174707-1 (2006).
- ² G. Thiault, A. Mellouki, G. Le Bras, A. Chakir, N. Sokolowski-Gomez, and D. Daumont, *J. Photochem. Photobio. A* 162, 273 (2004).
- ³ Y. Hirata and E. C. Lim, *J. Chem. Phys.* 72 (10), 5505 (1980).
- ⁴ T. Itoh, *Chem. Phys. Lett.* 133 (3), 254 (1987).
- ⁵ M. B. Robin and N. A. Kuebler, *J. Am. Chem. Soc.* 97 (17), 4822 (1975).
- ⁶ T. Itoh, H. Baba, and T. Takemura, *Bull. Chem. Soc. Jpn.* 51 (10), 2841 (1978).
- ⁷ N. Ohmori, T. Suzuki, and M. Ito, *J. Phys. Chem.* 92 (5), 1086 (1988).
- ⁸ E. Villa, A. Amirav, W. Chen, and E. C. Lim, *Chem. Phys. Lett.* 147 (1), 43 (1988).
- ⁹ A. Inoue and N. Ebara, *Chem. Phys. Lett.* 109 (1), 27 (1984).
- ¹⁰ M. Berger, I. L. Goldblatt, and C. Steel, *J. Am. Chem. Soc.* 95 (6), 1717 (1973).
- ¹¹ U. Brühlmann, M. Monella, P. Russegger, and J. R. Huber, *Chem. Phys.* 81, 439 (1983).
- ¹² C. R. Silva and J. P. Reilley, *J. Phys. Chem.* 100 (43), 17111 (1996).
- ¹³ M. Biron and P. Longin, *Chem. Phys. Lett.* 116 (2,3), 250 (1985).
- ¹⁴ T. Itoh, *Chem. Phys. Lett.* 151 (1,2), 166 (1988).
- ¹⁵ T. Itoh, T. Takemura, and H. Baba, *Chem. Phys. Lett.* 40 (3), 481 (1976).
- ¹⁶ M. Kiritani, T. Yoshii, N. Hirota, and M. Baba, *J. Phys. Chem.* 98 (44), 11265 (1994).
- ¹⁷ M. Koyanagi and L. Goodman, *Chem. Phys.* 39, 237 (1979).
- ¹⁸ O. Sneh and O. Cheshnovsky, *J. Phys. Chem.* 95 (19), 7154 (1991).
- ¹⁹ S.-H. Lee, K.-C. Tang, I.-C. Chen, M. Schmitt, J. P. Shaffer, T. Schultz, J. G. Underwood, M. Z. Zgierski, and A. Stolow, *J. Phys. Chem. A* 106 (39), 8979 (2002).

- 20 Y. Kanda, H. Kaseda, and T. Matamura, *Spectrochim. Acta* 20, 1387 (1964).
- 21 H. Murai and K. Obi, *J. Phys. Chem.* 79 (22), 2446 (1975).
- 22 S. Nagaoka and N. Hirota, *Bull. Chem. Soc. Jpn.* 56, 3381 (1983); L. Goodman
and M. Koyanagi, *Mol. Photochem.* 4 (3), 369 (1972).
- 23 I. Ozkan and L. Goodman, *Chem. Phys. Lett.* 64 (1), 32 (1979).
- 24 H. Hayashi and S. Nagakura, *Mol. Phys.* 27 (4), 969 (1974).
- 25 D. G. Leopold, R. J. Hemley, and V. Vaida, *J. Chem. Phys.* 75 (10), 4758 (1981).
- 26 L. Goodman and I. Ozkan, *Chem. Phys. Lett.* 61 (2), 216 (1979).
- 27 C. Mijoule and P. Yvan, *Chem. Phys. Lett.* 43 (3), 524 (1976); J. E. Ridley and M.
C. Zerner, *J. Mol. Spect.* 76, 71 (1979).
- 28 V. Molina and M. Merchán, *J. Phys. Chem. A* 105 (15), 3745 (2001).
- 29 W.-H. Fang and D. L. Phillips, *Chem. Phys. Chem.* 3 (10), 889 (2002).
- 30 Y.-W. Wang, H.-Y. He, and W.-H. Fang, *J. Mol. Struct. (THEOCHEM)* 634, 281
(2003).
- 31 R. K. Kakar, E. A. Rinehart, C. R. Quade, and T. Kojima, *J. Chem. Phys.* 52 (7),
3803 (1970).
- 32 K. B. Borisenko, C. W. Bock, and I. Hargittai, *J. Phys. Chem.* 100 (18), 7426
(1996).
- 33 V. S. Antonov, V. S. Letokhov, and A. N. Shibanov, *Appl. Phys.* 22, 293 (1980).
- 34 S. R. Long, J. T. Meek, P. J. Harrington, and J. P. Reilley, *J. Chem. Phys.* 78 (6),
3341 (1983).
- 35 J. J. Yang, D. A. Gobeli, and M. A. El-Sayed, *J. Phys. Chem.* 89 (15), 3426
(1985).
- 36 J. J. Yang, D. A. Gobeli, R. S. Pandolfi, and M. A. El-Sayed, *J. Phys. Chem.* 87
(12), 2255 (1983).
- 37 A. V. Polevoi, V. M. Matyuk, G. A. Grigor'eva, and V. K. Potapov, *Khim. Vys.
Énerg.* 18 (3), 195 (1984).
- 38 C. R. Silva and J. P. Reilley, *J. Phys. Chem. A* 101 (43), 7934 (1997).
- 39 L. Zhu and T. J. Cronin, *Chem. Phys. Lett.* 317, 227 (2000).

- 40 V. S. Antonov, I. N. Knyazev, V. S. Letokhov, V. M. Matyuk, V. G. Movshev,
and V. K. Potapov, *Khim. Vys. Énerg.* 12 (5), 476 (1978); V. S. Antonov and V.
S. Letokhov, *Appl. Phys.* 24, 89 (1981); V. S. Antonov, *Opt. Spektrosk.* 52, 10
(1982).
- 41 M. A. Grela and A. J. Colussi, *J. Phys. Chem.* 90 (3), 434 (1986).
- 42 J. A. Warren and E. R. Bernstein, *J. Chem. Phys.* 85 (5), 2365 (1986).
- 43 M. Koyanagi, R. J. Zwarich, and L. Goodman, *J. Chem. Phys.* 56 (6), 3044 (1972).
- 44 M. Berger and C. Steel, *J. Am. Chem. Soc.* 97 (17), 4817 (1975).
- 45 A. Inoue, M. Ushiyama, and N. Ebara, *Chem. Phys. Lett.* 117 (1), 18 (1985); A. R.
Rennert and C. Steel, *Chem. Phys. Lett.* 78 (1), 36 (1981); G. A. Zalesskaya, D. L.
Yakovlev, and E. G. Sambor, *Opt. Spektrosk.* 86 (2), 205 (1999).
- 46 Y. Hirata and E. C. Lim, *Chem. Phys. Lett.* 71 (1), 167 (1980).
- 47 A. P. Darmanyan and C. S. Foote, *J. Phys. Chem.* 97 (18), 4573 (1993).
- 48 A. P. Baronavski and J. C. Owrutsky, *Chem. Phys. Lett.* 333, 36 (2001).
- 49 J. Dobkowksi, Z. R. Grabowski, J. Waluk, W. Kühne, W. Rettig, C. Rullière, W.
Yang, J. Adamus, and J. Gebicki, *Proc. Indian Acad. Sci.* 104 (2), 143 (1992).
- 50 S. Srivistava, E. Yourd, and J. P. Toscano, *J. Am. Chem. Soc.* 120 (24), 6173
(1998).
- 51 S. Anand, M. M. Zamari, G. Menkir, R. J. Levis, and H. B. Schlegel, *J. Phys.*
Chem. A 108 (15), 3162 (2004).
- 52 H.-Q. Zhao, Y.-S. Cheung, C.-L. Liao, C.-X. Liao, C. Y. Ng, and W.-K. Li, *J.*
Chem. Phys. 107 (18), 7230 (1997).
- 53 H. Y. Afeefy, J. F. Liebman, and S. E. Stein, in *NIST Chemistry WebBook, NIST*
Standard Reference Database Number 69, edited by P. J. Linstrom and W. G.
Mallard (National Institute of Standards and Technology, Gaithersburg MD,
20899, June 2005).
- 54 A. B. Burrill, J. T. Zhou, and P. M. Johnson, *J. Phys. Chem. A* 107 (23), 4601
(2003).
- 55 D. G. Wilden and J. Comer, *J. Phys. B: Atom. Molec. Phys.* 13, 627 (1980).

- ⁵⁶ P. Swiderek, M. Michaud, and L. Sanche, *J. Chem. Phys.* 105 (16), 6724 (1996).
- ⁵⁷ E. Yamamoto, T. Yoshidome, T. Ogawa, and H. Kawazumi, *J. Elec. Spectr. and Rel. Phenom.* 63 (4), 341 (1993).
- ⁵⁸ H. Nakano, *J. Chem. Phys.* 99 (10), 7983 (1993).
- ⁵⁹ E. W.-G. Diau, C. Kötting, and A. H. Zewail, *Chem. Phys. Chem.* 2, 273 (2001).
- ⁶⁰ K. A. Holbrook, M. J. Pilling, and S. H. Robertson, *Unimolecular Reactions*, 2nd ed. (Wiley, New York, 1996).
- ⁶¹ W. H. Press, S. A. Teukolsky, W. T. Vetterling, and B. P. Flannery, *Numerical Recipes in C: the art of scientific computing*. (Cambridge University Press, Cambridge, 1999).
- ⁶² J. G. Calvert and J. N. Pitts Jr., *Photochemistry*. (Wiley, New York, 1967).
- ⁶³ A. Horowitz and J. G. Calvert, *J. Phys. Chem.* 86 (16), 3105 (1982); A. Horowitz, C. J. Kershner, and J. G. Calvert, *J. Phys. Chem.* 86 (16), 3094 (1982); J. S. Yadav and J. D. Goddard, *J. Chem. Phys.* 84 (5), 2682 (1986); Y. Kurosaki and K. Yokoyama, *Chem. Phys. Lett.* 371, 568 (2003).
- ⁶⁴ B. F. Gherman, R. A. Friesner, T.-H. Wong, Z. Min, and R. Bersohn, *J. Chem. Phys.* 114 (14), 6128 (2001).
- ⁶⁵ C. B. Moore and J. C. Weisshaar, *Ann. Rev. Phys. Chem.* 34, 525 (1983).
- ⁶⁶ R. G. W. Norrish, H. G. Crone, and O. D. Saltmarsh, *J. Chem. Soc.*, 1456 (1934).
- ⁶⁷ Y. Haas, *Photochem. Photobio. Sci.* 3, 6 (2004).
- ⁶⁸ W.-K. Chen, J.-W. Ho, and P.-Y. Cheng, *J. Phys. Chem. A* 109, 6805 (2005); W.-K. Chen and P.-Y. Cheng, *J. Phys. Chem. A* 109, 6818 (2005).
- ⁶⁹ Y. Kurosaki and K. Yokoyama, *J. Phys. Chem. A* 106 (47), 11415 (2002).